

Observation of a Fully-formed Forward–Reverse Shock Pair Due to the Interaction Between Two Coronal Mass Ejections at 0.5 au

DOMENICO TROTTA ¹, ANDREW DIMMOCK ², XOCHITL BLANCO-CANO ³, ROBERT FORSYTH ¹,
HELI HIETALA ⁴, NAIS FARGETTE ¹, ANDREA LAROSA ⁵, NOÉ LUGAZ ⁶, ERIKA PALMERIO ⁷,
SIMON W. GOOD ⁸, EMILIA K. J. KILPUA ⁸, EMILIYA YORDANOVA ², ORESTE PEZZI ⁵,
GEORGIOS NICOLAOU ⁹, TIMOTHY S. HORBURY ¹, RAMI VAINIO ¹⁰, NINA DRESING ¹⁰,
CHRISTOPHER J. OWEN ⁹ AND ROBERT F. WIMMER-SCHWEINGRUBER ¹¹

¹*The Blackett Laboratory, Department of Physics, Imperial College London, London SW7 2AZ, UK*

²*Swedish Institute of Space Physics, 751 21 Uppsala, Sweden*

³*Departamento de Ciencias Espaciales, Instituto de Geofísica, Universidad Nacional Autónoma de México, Ciudad Universitaria, 04150 Ciudad de México, Mexico*

⁴*Department of Physics and Astronomy, Queen Mary University of London, London E1 4NS, UK*

⁵*Istituto per la Scienza e Tecnologia dei Plasmi (ISTP), Consiglio Nazionale delle Ricerche, I-70126 Bari, Italy*

⁶*Space Science Center, University of New Hampshire, Durham, NH 03824, USA*

⁷*Predictive Science Inc., San Diego, CA 92121, USA*

⁸*Department of Physics, University of Helsinki, FI-00014 Helsinki, Finland*

⁹*Department of Space and Climate Physics, Mullard Space Science Laboratory, University College London, Dorking, Surrey, RH5 6NT, UK*

¹⁰*Department of Physics and Astronomy, University of Turku, FI-20014 Turku, Finland*

¹¹*Institute of Experimental and Applied Physics, Kiel University, D-24118 Kiel, Germany*

ABSTRACT

We report direct observations of a fast magnetosonic forward–reverse shock pair observed by Solar Orbiter on March 8, 2022 at the short heliocentric distance of 0.5 au. The structure, sharing some features with fully-formed stream interaction regions (SIRs), is due to the interaction between two successive coronal mass ejections (CMEs), never previously observed to give rise to a forward–reverse shock pair. The scenario is supported by remote observations from the STEREO-A coronagraphs, where two candidate eruptions compatible with the in-situ signatures have been found. In the interaction region, we find enhanced energetic particle activity, strong non-radial flow deflections and evidence of magnetic reconnection. At 1 au, well radially-aligned *Wind* observations reveal a complex event, with characteristic observational signatures of both SIR and CME–CME interaction, thus demonstrating the importance of investigating the complex dynamics governing solar eruptive phenomena.

Keywords: Sun: coronal mass ejections (CMEs) — Sun: heliosphere — (Sun:) solar wind

1. INTRODUCTION

The Sun is an active star, responsible for creating a highly complex and dynamic envi-

ronment in its surroundings, namely the heliosphere. The solar activity and global field struc-

tures manifest themselves in a broad range of temporal and spatial scales in the heliosphere.

The most common global structures that strongly influence the heliosphere are stream interaction regions (SIRs) and coronal mass ejections (CMEs). Understanding their origin and propagation is pivotal for a broad range of applications. Such phenomena play an important role in the production of energetic particles and in the overall heliosphere energetics (Rice et al. 2003). SIRs and CMEs also represent major drivers of the Sun–Earth interaction, making their investigation crucial from a space weather perspective (Temmer 2021).

SIRs form when the fast solar wind emerging from solar coronal holes interacts with the slow solar wind upstream of it (see Richardson 2018, for a review). SIRs are crucial for planetary space weather (Zhang et al. 2007), in particular for enhancing high energy particles fluxes in the Van Allen radiation belts (e.g., Kilpua et al. 2015). SIRs are the main source of heliospheric suprathermal particles at solar minimum, when they also play a major role in modulating cosmic ray activity (Heber & Burger 1999). SIRs are characterised by a region of compressed plasma, bounded by a pair of forward–reverse pressure waves, which can steepen into forward–reverse shocks, travelling away from and towards the Sun in the solar wind rest frame, respectively (Belcher 1971). At 1 au, it was shown that less than 1% of the SIRs are associated with forward–reverse shock pairs (Jian et al. 2006). Even fewer forward–reverse shock pairs are found in the inner heliosphere below 1 au, as shown by Schwenn (1996) using *Helios* observations. Using the Pioneer Venus Orbiter (PVO) observations, Jian et al. (2008) reported that SIR-related shocks are still very rare near Venus, at 0.73 AU.

CMEs are the largest eruptive events from the Sun, defined as an observable change in the coronal structure and an outward motion away

from the Sun (Schwenn 1996). They propagate at large heliocentric distances, and their rate is proportional to solar activity. CMEs are excellent systems of energy conversion, from the release of magnetic energy at their origin to the shock-mediated conversion bulk flow energy into heat and energetic particles during their propagation (Chen 2011). In-situ, CMEs show characteristic observable signatures and are often separated in a forward shock (not always present), a compressed sheath region, and magnetic ejecta (Kilpua et al. 2017). Forward–reverse shock pairs due to transient disturbances and CMEs were also reported at 1 au using early International Sun–Earth Explorer (ISEE) observations (Gosling et al. 1988).

Increased solar activity introduces the opportunity to study the interaction between multiple CMEs, which may happen in a variety of ways with different in-situ signatures (see Lugaz et al. 2017, for a review). Multiple-CME events may lead to intense geomagnetic storms (Scolini et al. 2020; Koehn et al. 2022) and extremely intense solar energetic particle (SEP) events (Zhuang et al. 2020). Interacting CMEs are the object of flourishing scientific debate, establishing their role in heliospheric energetics (Lugaz & Farrugia 2014; Palmerio et al. 2021).

The Sun is approaching the maximum activity of solar cycle 25, and novel datasets are now available, due to the ground-breaking Parker Solar Probe (PSP, Fox et al. 2016) and Solar Orbiter (Müller, D. et al. 2020) missions. Thus, a novel observational window for solar eruptive phenomena has opened (e.g., Dresing, N. et al. 2023; Trotta et al. 2024).

In this work, we exploit this new window by reporting, for the first time, a fully formed forward–reverse shock pair driven by two interacting CMEs. The shock pair is observed by Solar Orbiter as close to the Sun as 0.5 au on March 8, 2022. We identi-

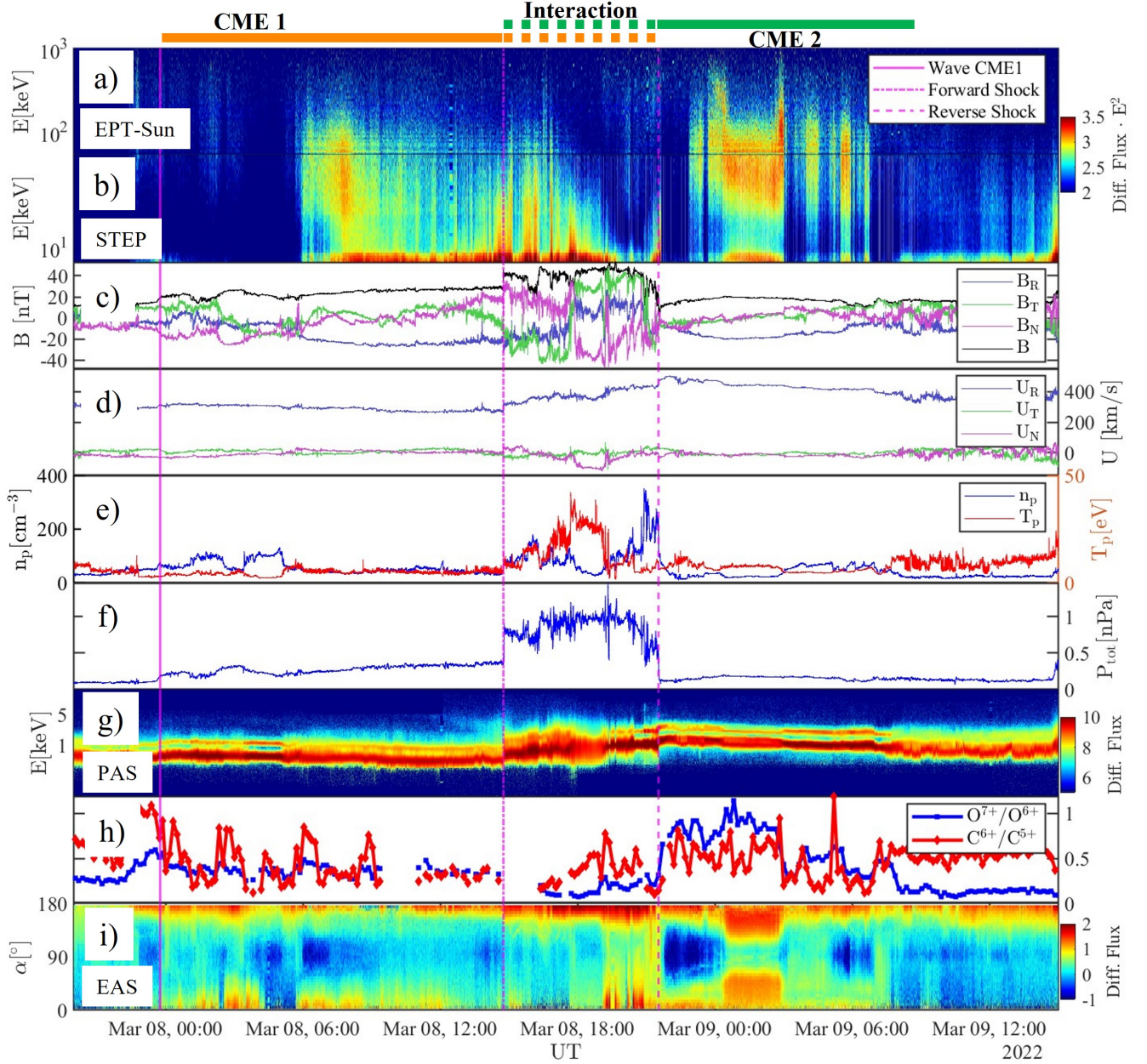


Figure 1. Summary of Solar Orbiter observations. a-b): Energetic differential fluxes (in $E^2 \cdot \text{cm}^{-2}\text{s}^{-1}\text{sr}^{-1}\text{MeV}$) as measured from EPD's Sun-directed Electron Proton Telescope (EPT, a) and Supra Thermal Electron Proton sensor (STEP, b). c) MAG normal mode magnetic field magnitude and components in RTN. d-e) Proton bulk flow speed, proton density and temperature as measured by SWA-PAS (Proton Alpha Sensor). f) Plasma total pressure ($P_{\text{tot}} = n_p k_B T_p + \frac{B^2}{2\mu_0}$ where k_B and μ_0 are the Boltzmann constant and the vacuum magnetic permeability). g) One-dimensional energy flux (in $\text{cm}^{-2}\text{s}^{-1}\text{eV}$) measured by PAS. h) Element abundance ratios measured by the SWA Heavy Ion Sensor (HIS). i) Integrated pitch angle distributions for electrons with energies larger than 100 eV as measured by SWA-Electron Analyser Sensor (EAS) (in $\text{cm}^{-2}\text{s}^{-1}\text{eV}$). The continuous, dashed-dotted and dashed lines show the times at which Solar Orbiter crosses the CME1 wave, the forward and reverse shock, respectively.

fied two candidate CMEs coronagraph images from the Solar Terrestrial Relations Observatory (STEREO; Kaiser et al. 2008) and finally studied their evolution using the well radially-aligned *Wind* (Ogilvie & Desch 1997) spacecraft at 1 au. We describe the data products used in Section 2, while the results are presented in Section 3, and the conclusions reported in Section 4.

2. DATA

We use STEREO-A’s Sun Earth Connection Coronal and Heliospheric Investigation (SECCHI; Howard et al. 2008) suite, with focus on the COR2 coronagraph, imaging the solar atmosphere up to $15 R_{\odot}$.

At Solar Orbiter, we use the flux-gate magnetometer (MAG; Horbury et al. 2020). Ion moments and suprathermal electron pitch angle distributions and composition are from the Solar Wind Analyser suite (SWA; Owen et al. 2020). Energetic particles have been measured by the Energetic Particle Detector (EPD; Rodríguez-Pacheco, J. et al. 2020).

From *Wind*, we use the Magnetic Field Investigation (MFI; Lepping et al. 1995), and the Three-Dimensional Plasma and Energetic Particle Investigation (3DP; Lin et al. 1995) instrument for ion moments and electron distributions.

3. RESULTS

On March 8, 2022, Solar Orbiter crossed a forward–reverse shock pair at 0.49 au (Figure 1). The time separation between the two shocks is 6 hours and 47 minutes.

The shock parameters, computed using the SerPyShock package (Trotta et al. 2022), systematically changing the upstream/downstream averaging windows from a few seconds to 2 minutes, are summarized in Table 1. The forward shock is oblique ($\theta_{Bn} \sim 60^\circ$), with small Mach numbers, while the reverse shock more perpendicular and stronger, compatible with previ-

ous studies of SIR shocks (Kilpua et al. 2015). Both shocks exhibit an interesting small-scale behaviour, which will be part of a follow-up work.

Figure 1 shows an overview of the event, with the forward–reverse shock pair highlighted by the dashed magenta lines. The interaction region between the shocks resembles a fully-formed SIR (see, e.g., Richardson 2018), more often observed at 1 au and beyond. It is associated with a magnetic field compression, two subsequent increases in the bulk flow speed, and enhanced total plasma pressure (Figure 1c, d, f).

Further analysis of the event reveals that the forward–reverse shock pair is not created in the interaction between fast and slow wind, but rather between two CMEs (CME1 and CME2 in chronological order, see Figure 1) with different propagation speeds (about 290 and 450 km/s, respectively). This is readily seen by the presence of several clear indicators of the CME material (see Zurbuchen et al. 2016) both before and after the interaction region, including the smooth magnetic field rotations upstream/downstream of the interaction, the enhanced O^{7+}/O^{6+} ratios and the bi-directional pitch angle distributions of suprathermal electrons (Figure 1c,h,i). Figure 1 shows that the CME1 is both slower (Figure 1 d) and possibly magnetically less well-connected to the Sun (less clear bidirectional electron). The start of CME1, on March 7, 2022, 7:23:46 UT, magenta line in Figure 1 has not steepened into a shock due to the slow CME1 propagation speed. Downstream of the CME1 wave, we observe a change of parameters (around 6:00 UT on March 8), marking the start of enhanced energetic particle fluxes within the CME1 ejecta (Figure 1 a, b). Protons with energies of up to 7 MeV were found, irregularly distributed within both the CME1 and CME2 ejecta and in the interaction region. This behaviour may de-

Table 1. Shock times and parameters inferred from Solar Orbiter direct observations. The parameters shown are (left to right): shock normal vector, θ_{Bn} , magnetic compression ratio r_B , gas compression ratio r , shock speed v_{sh} , upstream plasma beta β_{up} , fast magnetosonic and Alfvénic Mach numbers (M_{fms} and M_A , respectively).

Shock	Time [UT]	$\langle \hat{n}_{RTN} \rangle$	$\langle \theta_{Bn} \rangle$ [°]	$\langle r_B \rangle$	$\langle r \rangle$	$\langle v_{sh} \rangle$ [km/s]	β_{up}	M_{fms}	M_A
Forward	08-Mar-2022 14:04:26	[0.95 -0.11 0.30]	59	1.5	2	367	0.09	1.2	1.1
Reverse	08-Mar-2022 21:33:01	[-0.94 0.15 0.32]	69	2	2.1	-373	3.1	2	3.8

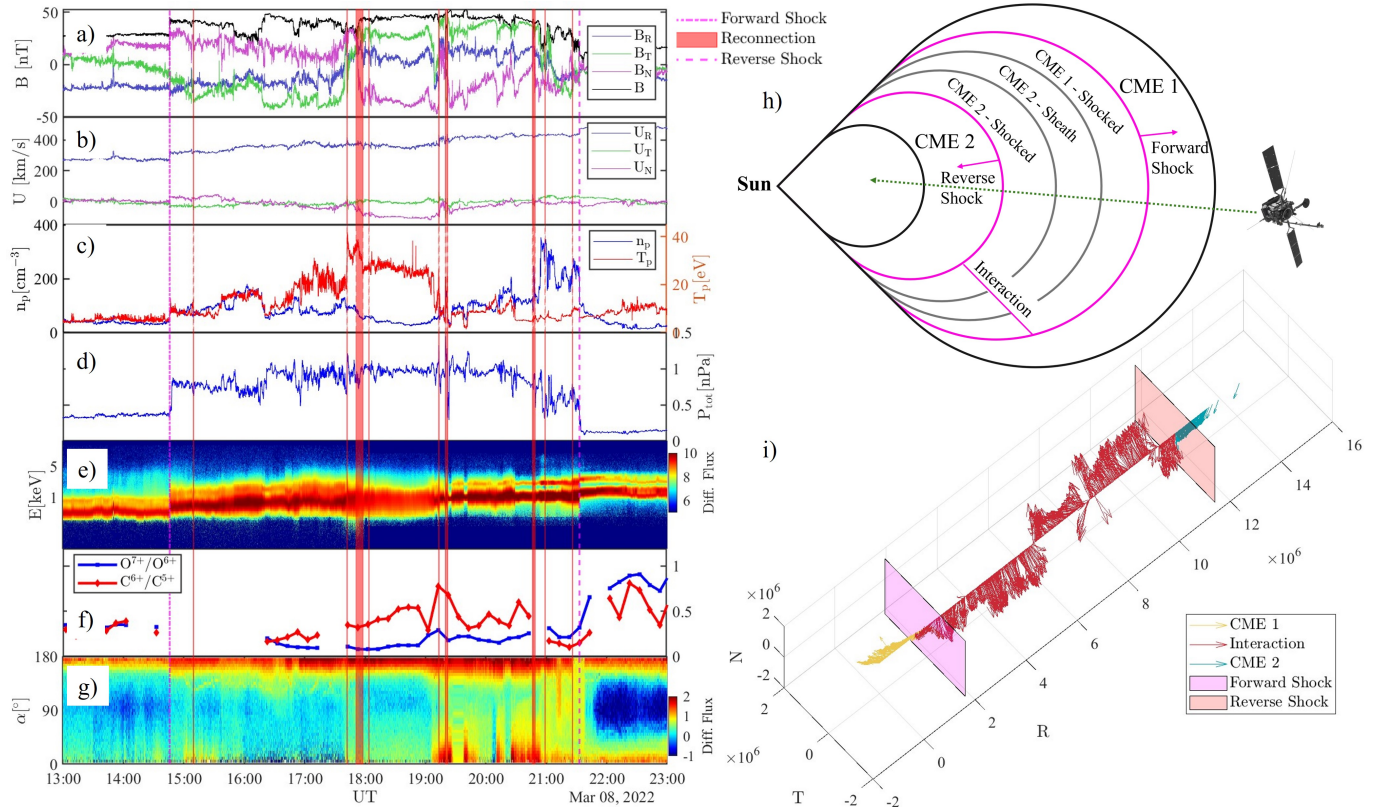


Figure 2. a-g: Zoom on the interaction region as in Figure 1 without the energetic particles spectrogram. h: Simplified sketch representing the event with the identified areas within the interaction and the Solar Orbiter trajectory (spacecraft model: esa.com). i: Three-dimensional plot of magnetic field vectors in RTN for the event. Yellow, red and blue arrows are measurements taken in CME1, interaction and CME2 regions, respectively. The magenta/orange planes represent the forward-reverse shock pair.

pend on the intrinsic complexity of the environment measured. Furthermore complexity may be due to further injection of energetic particles at the Sun, where we identified a type III radio burst at 4:30 UT (not shown here). Starting at about 13:00 UT, we report enhanced particle fluxes upstream of and well-connected to the forward shock, readily seen in at high ener-

gies in the spectrogram in Figure 1g. This extended particle foreshock propagating in CME1 and thereby producing foreshock waves will be object of further study.

We focus on the interaction region properties, showing a zoom of the Solar Orbiter measurements and a simplified sketch of the event in Figure 2. The trailing part of the interaction re-

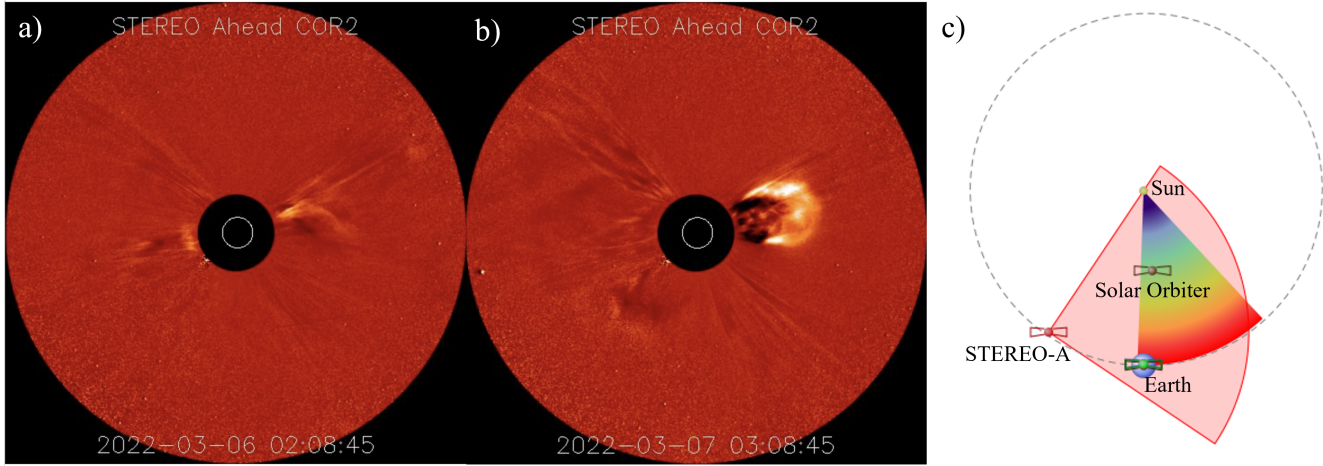


Figure 3. a–b): Two successive eruptions as observed by the STEREO-A COR2 coronagraph. c) Orbital configuration at the start time of the interaction. The STEREO-A heliospheric imager field of view and a model CME propagation compatible with observations in b) have been superimposed (red and colored cones, respectively).

gion is characterised by higher plasma densities, lower temperatures, and higher elemental abundances (Figure 2 f) than the leading portion. The pitch angle distributions show that magnetic connectivity changes in the end portion of the interaction region from field lines connected to the Sun at one end to those having both ends connected. These observations emphasise that the interaction region consists of plasma from two different sources.

The interaction region shows sub-structuring, with irregular behaviour in many measured quantities (Figure 2 left). We suggest that this is due to the spacecraft probing, in rapid succession, the material at the end of CME1, and material in the CME2 sheath and cloud (Figure 2h), as particularly evident in the plasma signatures (Figure 2 c, e). Plasma belonging to different regions may mix due to reconnection, discussed below.

The leading part of the interaction region is characterised by hot plasma, strongly processed by the forward shock. Progressing through the interaction, we observe abrupt changes in magnetic field direction, in association with strong transverse flow deflections (at 18:00 and 19:05 UT), corresponding to plasma being de-

flected away from the radial direction in the interaction between the two events. We interpret this region as the interface between the two CMEs.

As done in observations of planar magnetic structures in the solar wind (e.g., Nakagawa et al. 1989) and in CME-driven sheath regions (Palmerio et al. 2016), we applied a Minimum Variance Analysis (MVA) to the magnetic field in the interaction region. In the interval from the immediate downstream of the forward shock to the reverse shock, the intermediate-to-minimum eigenvalue ratio of the MVA matrix is large $\lambda_2/\lambda_3 \sim 8$. This implies the existence of a well-defined minimum variance direction. Projecting the magnetic field components in the MVA frame highlights the change at the interface region at 18:00 UT mentioned above (not shown here). Strong changes at 19:00 UT are also found both with the MVA and magnetic reconnection diagnostics (see below), indicating that there may be more than one interface crossing.

Further characterization was performed, searching for magnetic reconnection signatures, crucial for mixing plasmas efficiently (e.g., Russell et al. 1990). We used the magnetic recon-

nection method successfully applied to Solar Orbiter data in Fargette et al. (2023). Orange shaded regions in Figure 2 (left) correspond to reconnection exhaust crossings. It is readily seen that the interaction region undergoes strong reconnection activity, very long-lasting around 18:00 UT, corresponding to the previously identified CME–CME interface and corroborating the interpretation of complex mixing of CMEs.

Finally, in Figure 2i we show a three-dimensional plot of the magnetic field vectors as measured by Solar Orbiter in the CME1, interaction region, and CME2 intervals (yellow, red, and teal arrows, respectively), with the forward–reverse shock pair represented as the magenta/orange planes, respectively. The interface between the two CMEs can be clearly seen in the sharp change of direction of the magnetic field.

The spacecraft orbital configuration during the event makes it possible to get unique insights about the evolution of this novel interaction structure. Using the COR2 coronagraph of the STEREO-A spacecraft, we identified two candidate eruptions from the Sun, possibly the progenitors of the observed interaction. These are displayed in Figure 3 a, b for CME1 and CME2, respectively, while Figure 3 c shows the spacecraft orbital configuration with the STEREO-A field of view (red cone) and a model CME eruption (rainbow cone) obtained using the propagation tool in Rouillard et al. (2017). While the identification for the remote counterparts of CME1 and CME2 is not straightforward, both candidates are compatible with the direction of the eruption and their arrival time at Solar Orbiter. Such remote observations highlight how even “faint” solar eruptions can give rise to energetic events through complex interaction.

During the event, the Solar Orbiter–Earth longitudinal separation was about 9° . We ex-

ploited the configuration and We found an in-situ structure crossing the *Wind* spacecraft at the Sun–Earth Lagrange point L1 at 13:00 UT on March 10, 2023, compatible with the Solar Orbiter event propagating at about 400 km s^{-1} speed from 0.5 to 1 au.

In Figure 4, it is readily noted that the forward–reverse shock pair is not present at *Wind*. Only a fast forward shock is observed at *Wind* ahead of the whole structure, crossing the spacecraft on March 10 at 16:11:32 UTC. The shock has a complex magnetic structure upstream and downstream and a data gap in plasma measurements immediately downstream, making shock parameter estimation particularly difficult. However, we estimate that the shock is oblique ($\theta_{Bn} \sim 55^\circ$) and the Alfvén Mach number is very low, close to 1.

The event at *Wind* is compatible with the complex ejecta resulting from the interaction of multiple CMESs, as reported in Lugaz et al. (2017), with some differences, such as high density and temperature ejecta. The structure, at 1 au, has also some features reminiscent of a SIR (e.g., magnetic compression), but missing the typical fast stream signature corresponding to the reverse pressure wave. We note that the solar wind speed is slower in the first portion of the complex ejecta than in the second, thus maintaining the general trends of the structure at Solar Orbiter. It is also possible that the 10° separation between the two locations was sufficient to measure different parts of the event between Solar Orbiter and L1. Therefore, these joint observations highlight the transient nature of this novel interaction. Indeed, the interaction has weakened from 0.5 to 1 au, in contrast with what expected from SIR driven forward–reverse shock pairs that tend to get stronger as they move to high heliocentric distances (Richardson et al. 2022). The event was not found to cause any major space weather disturbance at Earth, consistent with the lack of periods

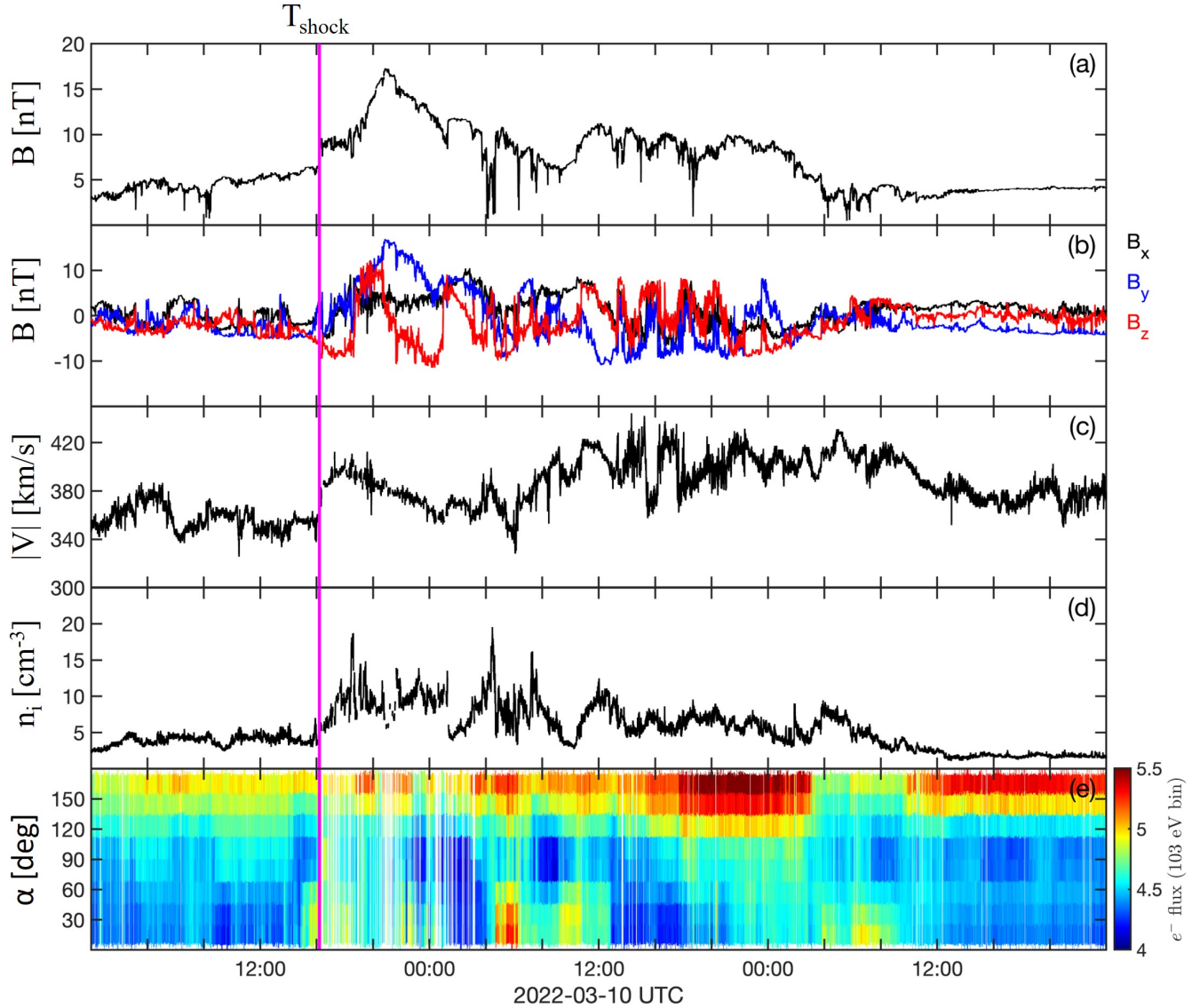


Figure 4. *Wind* observations for the event at 1 au. From top to bottom are displayed: magnetic field magnitude and components in the Geocentric Solar Ecliptic (GSE) frame, ion bulk flow speed, ion density and suprathermal 103 eV electron pitch angle spectrograms. The magenta line marks the forward shock crossing.

with steady magnetic field orientations (Dimmock et al. 2019).

4. CONCLUSIONS

We reported direct observations of a fully-formed reverse-forward shock pair at the very low heliocentric distance of 0.5 au. While such a shock pair is typically associated with an SIR, it was found to be originated from the interaction between a fast and a slow CME. To our

knowledge, this is the first time that such an observation is reported.

The CME-CME interaction drives a complex compression region, where the interface separates the plasma from two different sources and is characterised by a high-level of magnetic reconnection activity and several irregularities in the measured plasma conditions. Such characterisation underlines the role of this structure in

creating favourable conditions efficient energy dissipation (Richardson 2018).

Energetic ions up to several MeV were observed, with a strongly irregular behaviour, influenced by the complex plasma environment, stimulating an advancement of knowledge for energetic particle behaviour in the heliosphere. On one hand, due to novel, high time-energy resolution of energetic particles datasets (see Wimmer-Schweingruber, R. F. et al. 2021), we were able to link irregular particle behaviour, to the plasma irregularities (discontinuities, reconnection) present in the same region, a study in continuity with others using EPD in different environments (e.g. Trotta et al. 2023). On the other hand, it was shown that a significant amount of high energy (~ 7 MeV) particles may be generated in the interaction between weak eruptive events, with important consequences for ongoing modelling efforts in SEP acceleration and propagation (e.g. Ding et al. 2024; Zhuang et al. 2022).

The forward–reverse shock pair propagating in CME material also offers opportunity to study shock micro-physics in unusual ambient parameters, as in the case of the forward shock exhibiting an extended particle foreshock despite the very low Mach number, probably due to the low level of upstream magnetic field fluctuations of CME1 (see Lario et al. 2022; Trotta et al. 2021). Studying shock behaviour in this poorly explored parameter space is important for the astrophysical implications of this research, and will be object of further studies.

This study exploited the unique orbital configuration during the event, with two remote CME candidates identified using the STEREO-A coronagraph. These observations highlighted the importance of connecting remote and direct observations, particularly as the first, slow CME was particularly faint and yet it gave rise to such an interesting event.

We also investigated the evolution of this structure also at 1 au using the *Wind* spacecraft, revealing a merged structure without forward–reverse shock pair and mixed features between a CME and SIR event. This is in contrast with SIR–related shock pairs, which get more intense with heliospheric distance. The fact that such CME–CME related shock pairs seem to weaken with heliocentric distance is compatible with the fact that they have not been identified previously, and with earlier simulation studies of interacting CMEs (Lugaz et al. 2005).

To get further insights into the evolution of these transient, complex interactions has relevant implications to space weather events (Möstl et al. 2020), and will be further investigated exploiting the extended spacecraft fleet orbiting the inner heliosphere.

5. ACKNOWLEDGMENTS

This study has received funding from the European Unions Horizon 2020 research and innovation programme under grant agreement no. 101004159 (SERPENTINE, www.serpentine-h2020.eu). Views and opinions expressed are, however, those of the authors only and do not necessarily reflect those of the European Union or the European Research Council Executive Agency. Neither the European Union nor the granting authority can be held responsible for them. This work was supported by the UK Science and Technology Facilities Council (STFC) grant ST/W001071/1. Solar Orbiter magnetometer operations are funded by the UK Space Agency (grant ST/X002098/1). Solar Orbiter is a space mission of international collaboration between ESA and NASA, operated by ESA. Solar Orbiter Solar Wind Analyser (SWA) data are derived from scientific sensors which have been designed and created, and are operated under funding provided in numerous contracts from the UK Space Agency (UKSA), the UK Science and Tech-

nology Facilities Council (STFC), the Agenzia Spaziale Italiana (ASI), the Centre National d'Etudes Spatiales (CNES, France), the Centre National de la Recherche Scientifique (CNRS, France), the Czech contribution to the ESA PRODEX programme and NASA. Solar Orbiter SWA work at UCL/MSSL is currently funded under STFC grants ST/W001004/1 and ST/X/002152/1. H.H. is supported by the Royal Society University Research Fellowship URF\R1\180671. E.P. acknowledges support from NASA's Heliophysics Guest Investigators-Open programme (grant no. 80NSSC23K0447). S.W.G. is supported by the Research Council of Finland (INERTUM, grant no. 346612). N.D. acknowledges the support by the Research

Council of Finland (SHOCKSEE, grant no. 346902). E.Y. is supported by Swedish National Space Agency (grant no. 192/20). XBC is supported by DGAPA- PAPIIT grant IN106724. AL and OP are supported by the PRIN 2022 project "2022KL38BK - The ULtimate fate of TuRbulence from space to laboratory pLAsmas (ULTRA)" (Master CUP B53D23004850006) by the Italian Ministry of University and Research, funded under the National Recovery and Resilience Plan (NRRP), Mission 4 – Component C2 – Investment 1.1, "Fondo per il Programma Nazionale di Ricerca e Progetti di Rillevante Interesse Nazionale (PRIN 2022)" (PE9) by the European Union – NextGenerationEU.

AL acknowledges the support of the STFC Consolidated Grant ST/T00018X/1.

REFERENCES

- Belcher, J. W. 1971, *ApJ*, 168, 509, doi: [10.1086/151105](https://doi.org/10.1086/151105)
- Chen, P. F. 2011, *Living Reviews in Solar Physics*, 8, 1, doi: [10.12942/lrsp-2011-1](https://doi.org/10.12942/lrsp-2011-1)
- Dimmock, A. P., Rosenqvist, L., Hall, J.-O., et al. 2019, *Space Weather*, 17, 989, doi: <https://doi.org/10.1029/2018SW002132>
- Ding, Z., Li, G., Wijzen, N., Poedts, S., & Yao, S. 2024, *The Astrophysical Journal Letters*, 964, L8, doi: [10.3847/2041-8213/ad2f3c](https://doi.org/10.3847/2041-8213/ad2f3c)
- Dresing, N., Rodríguez-García, L., Jebaraj, I. C., et al. 2023, *A&A*, 674, A105, doi: [10.1051/0004-6361/202345938](https://doi.org/10.1051/0004-6361/202345938)
- Fargette, N., Lavraud, Benoît, Rouillard, Alexis P., et al. 2023, *A&A*, 674, A98, doi: [10.1051/0004-6361/202346043](https://doi.org/10.1051/0004-6361/202346043)
- Fox, N. J., Velli, M. C., Bale, S. D., et al. 2016, *SSRv*, 204, 7, doi: [10.1007/s11214-015-0211-6](https://doi.org/10.1007/s11214-015-0211-6)
- Gosling, J. T., Bame, S. J., Smith, E. J., & Burton, M. E. 1988, *Journal of Geophysical Research: Space Physics*, 93, 8741, doi: <https://doi.org/10.1029/JA093iA08p08741>
- Heber, B., & Burger, R. A. 1999, in *Corotating Interaction Regions*, ed. A. Balogh, J. T. Gosling, J. R. Jokipii, R. Kallenbach, & H. Kunow, Vol. 7 (Springer), 125–138, doi: [10.1007/978-94-017-1179-1_10](https://doi.org/10.1007/978-94-017-1179-1_10)
- Horbury, T. S., O'Brien, H., Carrasco Blazquez, I., et al. 2020, *Astronomy & Astrophysics*, 642, A9, doi: [10.1051/0004-6361/201937257](https://doi.org/10.1051/0004-6361/201937257)
- Howard, R. A., Moses, J. D., Vourlidas, A., et al. 2008, *SSRv*, 136, 67, doi: [10.1007/s11214-008-9341-4](https://doi.org/10.1007/s11214-008-9341-4)
- Jian, L., Russell, C., Luhmann, J., & Skoug, R. 2008, *Advances in Space Research*, 41, 259, doi: <https://doi.org/10.1016/j.asr.2007.03.023>
- Jian, L., Russell, C. T., Luhmann, J. G., & Skoug, R. M. 2006, *SoPh*, 239, 337, doi: [10.1007/s11207-006-0132-3](https://doi.org/10.1007/s11207-006-0132-3)
- Kaiser, M. L., Kucera, T. A., Davila, J. M., et al. 2008, *SSRv*, 136, 5, doi: [10.1007/s11214-007-9277-0](https://doi.org/10.1007/s11214-007-9277-0)
- Kilpua, E., Koskinen, H. E. J., & Pulkkinen, T. I. 2017, *Living Reviews in Solar Physics*, 14, 5, doi: [10.1007/s41116-017-0009-6](https://doi.org/10.1007/s41116-017-0009-6)
- Kilpua, E. K., Lumme, E., Andreeova, K., Isavnin, A., & Koskinen, H. E. 2015, *Journal of Geophysical Research: Space Physics*, 120, 4112, doi: [10.1002/2015JA021138](https://doi.org/10.1002/2015JA021138)
- Kilpua, E. K. J., Hietala, H., Turner, D. L., et al. 2015, *Geophys. Res. Lett.*, 42, 3076, doi: [10.1002/2015GL063542](https://doi.org/10.1002/2015GL063542)

- Koehn, G. J., Desai, R. T., Davies, E. E., et al. 2022, *The Astrophysical Journal*, 941, 139, doi: [10.3847/1538-4357/aca28c](https://doi.org/10.3847/1538-4357/aca28c)
- Lario, D., Richardson, I. G., Wilson, L. B., I., et al. 2022, *ApJ*, 925, 198, doi: [10.3847/1538-4357/ac3c47](https://doi.org/10.3847/1538-4357/ac3c47)
- Lepping, R. P., Acuña, M. H., Burlaga, L. F., et al. 1995, *SSRv*, 71, 207, doi: [10.1007/BF00751330](https://doi.org/10.1007/BF00751330)
- Lin, R. P., Anderson, K. A., Ashford, S., et al. 1995, *SSRv*, 71, 125, doi: [10.1007/BF00751328](https://doi.org/10.1007/BF00751328)
- Lugaz, N., & Farrugia, C. J. 2014, *Geophysical Research Letters*, 41, 769, doi: [10.1002/2013GL058789](https://doi.org/10.1002/2013GL058789)
- Lugaz, N., Manchester, W. B., I., & Gombosi, T. I. 2005, *ApJ*, 634, 651, doi: [10.1086/491782](https://doi.org/10.1086/491782)
- Lugaz, N., Temmer, M., Wang, Y., & Farrugia, C. J. 2017, *SoPh*, 292, 64, doi: [10.1007/s11207-017-1091-6](https://doi.org/10.1007/s11207-017-1091-6)
- Müller, D., St. Cyr, O. C., Zouganelis, I., et al. 2020, *A&A*, 642, A1, doi: [10.1051/0004-6361/202038467](https://doi.org/10.1051/0004-6361/202038467)
- Möstl, C., Weiss, A. J., Bailey, R. L., et al. 2020, *The Astrophysical Journal*, 903, 92, doi: [10.3847/1538-4357/abb9a1](https://doi.org/10.3847/1538-4357/abb9a1)
- Nakagawa, T., Nishida, A., & Saito, T. 1989, *Journal of Geophysical Research: Space Physics*, 94, 11761, doi: [https://doi.org/10.1029/JA094iA09p11761](https://doi.org/https://doi.org/10.1029/JA094iA09p11761)
- Ogilvie, K. W., & Desch, M. D. 1997, *Advances in Space Research*, 20, 559, doi: [10.1016/S0273-1177\(97\)00439-0](https://doi.org/10.1016/S0273-1177(97)00439-0)
- Owen, C. J., Bruno, R., Livi, S., et al. 2020, *Astronomy & Astrophysics*, 642, doi: [10.1051/0004-6361/201937259](https://doi.org/10.1051/0004-6361/201937259)
- Palmerio, E., Kilpua, E. K. J., & Savani, N. P. 2016, *Annales Geophysicae*, 34, 313, doi: [10.5194/angeo-34-313-2016](https://doi.org/10.5194/angeo-34-313-2016)
- Palmerio, E., Nieves-Chinchilla, T., Kilpua, E. K. J., et al. 2021, *Journal of Geophysical Research: Space Physics*, 126, e2021JA029770, doi: [10.1029/2021JA029770](https://doi.org/10.1029/2021JA029770)
- Rice, W. K. M., Zank, G. P., & Li, G. 2003, *Journal of Geophysical Research: Space Physics*, 108, doi: [https://doi.org/10.1029/2002JA009756](https://doi.org/https://doi.org/10.1029/2002JA009756)
- Richardson, I. G. 2018, *Living Reviews in Solar Physics*, 15, 1, doi: [10.1007/s41116-017-0011-z](https://doi.org/10.1007/s41116-017-0011-z)
- Richardson, J. D., Burlaga, L. F., Elliott, H., et al. 2022, *SSRv*, 218, 35, doi: [10.1007/s11214-022-00899-y](https://doi.org/10.1007/s11214-022-00899-y)
- Rodríguez-Pacheco, J., Wimmer-Schweingruber, R. F., Mason, G. M., et al. 2020, *A&A*, 642, A7, doi: [10.1051/0004-6361/201935287](https://doi.org/10.1051/0004-6361/201935287)
- Rouillard, A. P., Lavraud, B., Génot, V., et al. 2017, *Planet. Space Sci.*, 147, 61, doi: [10.1016/j.pss.2017.07.001](https://doi.org/10.1016/j.pss.2017.07.001)
- Russell, C. T., Priest, E. R., & Lee, L. C. 1990, *Geophysical Monograph Series*, 58, doi: [10.1029/GM058](https://doi.org/10.1029/GM058)
- Schwenn, R. 1996, *Ap&SS*, 243, 187, doi: [10.1007/BF00644053](https://doi.org/10.1007/BF00644053)
- Scolini, C., Chané, E., Temmer, M., et al. 2020, *ApJS*, 247, 21, doi: [10.3847/1538-4365/ab6216](https://doi.org/10.3847/1538-4365/ab6216)
- Temmer, M. 2021, *Living Reviews in Solar Physics*, 18, 4, doi: [10.1007/s41116-021-00030-3](https://doi.org/10.1007/s41116-021-00030-3)
- Trotta, D., Valentini, F., Burgess, D., & Servidio, S. 2021, *Proceedings of the National Academy of Sciences*, 118, e2026764118, doi: [10.1073/pnas.2026764118](https://doi.org/10.1073/pnas.2026764118)
- Trotta, D., Vuorinen, L., Hietala, H., et al. 2022, *Frontiers in Astronomy and Space Sciences*, 9, doi: [10.3389/fspas.2022.1005672](https://doi.org/10.3389/fspas.2022.1005672)
- Trotta, D., Horbury, T. S., Lario, D., et al. 2023, *The Astrophysical Journal Letters*, 957, L13, doi: [10.3847/2041-8213/ad03f6](https://doi.org/10.3847/2041-8213/ad03f6)
- Trotta, D., Larosa, A., Nicolaou, G., et al. 2024, *The Astrophysical Journal*, 962, 147, doi: [10.3847/1538-4357/ad187d](https://doi.org/10.3847/1538-4357/ad187d)
- Wimmer-Schweingruber, R. F., Janitzek, N. P., Pacheco, D., et al. 2021, *A&A*, 656, A22, doi: [10.1051/0004-6361/202140940](https://doi.org/10.1051/0004-6361/202140940)
- Zhang, J., Richardson, I. G., Webb, D. F., et al. 2007, *Journal of Geophysical Research: Space Physics*, 112, doi: [https://doi.org/10.1029/2007JA012321](https://doi.org/https://doi.org/10.1029/2007JA012321)
- Zhuang, B., Lugaz, N., Gou, T., Ding, L., & Wang, Y. 2020, *ApJ*, 901, 45, doi: [10.3847/1538-4357/abaef9](https://doi.org/10.3847/1538-4357/abaef9)
- Zhuang, B., Lugaz, N., & Lario, D. 2022, *The Astrophysical Journal*, 925, 96, doi: [10.3847/1538-4357/ac3af2](https://doi.org/10.3847/1538-4357/ac3af2)
- Zurbuchen, T. H., Weberg, M., von Steiger, R., et al. 2016, *The Astrophysical Journal*, 826, 10, doi: [10.3847/0004-637X/826/1/10](https://doi.org/10.3847/0004-637X/826/1/10)